NUCL SCI TECH (2022) 33:69
https://doi.org/10.1007/s41365-022-01064-4

Conceptual design and neutronic analysis of a megawatt-level vehicular microreactor based on TRISO fuel particles and S-CO_2 direct power generation

Fang-Yuan Zhang[1,2] · Gui-Feng Zhu[1,2] · Yang Zou[1,2] · Rui Yan[1,2] · Hong-Jie Xu[1,2]

Received: 22 December 2021 / Revised: 12 April 2022 / Accepted: 7 May 2022 / Published online: 2 July 2022

Abstract With global warming, the demand for diversified energy sources has increased significantly. Transportable microreactors are important potential supplements to the global power market and are a promising development direction. This paper describes a 5 MW integrated long-life S-CO_2 cooled vehicular microreactor (VMR) design based on tristructural isotropic (TRISO) fuel particles that aims to provide electricity for industrial power facilities, remote mines, and remote mountainous areas that are not connected to central power grids. First, to facilitate transportation, flexible deployment, and simplified operation and maintenance requirements, the VMR core and auxiliary system were designed to be reasonably small and as simple as possible. Second, the TRISO fuel particles used in the proposed VMR offer excellent properties, such as high inherent security and nonproliferation, which are vital for reactors in remote areas. In addition, a long core lifetime was achieved using the compact core design and enhanced fuel loading capacity, which is challenging when using TRISO as fuel. Finally, to make the VMR economically competitive in terms of improved neutron performance and fuel efficiency compared to similar designs, large-size TRISO particles and tube-in-duct fuel assembly were utilized and different core configurations were schemed and simulated to obtain the design that best satisfied the proposed criteria. The lifetime and burnup in the final optimized VMR were satisfactory at 21 years and 43.9 MWd/kgU, respectively, with an adequate shutdown margin and excellent safety parameters to ensure safe operation.

Keywords Vehicular microreactor · Tristructural isotropic particle · Tube-in-duct assembly · Compact core · Lifetime · Burnup

1 Introduction

The Advanced Research Projects Agency-Energy (ARPA-E) DOE defines a reactor with an output power of 10 MWe or less as a micromodular reactors [1]. Microreactors have the characteristics of small size, high flexibility, strong adaptability, and multipurpose design, which can provide great economic benefits through series production. The main application scenarios of microreactors are in deep sea, space, and remote areas.

Transportable microreactors have great research potential and can be traced back to the 1960s, when the USA started research on transportable microreactors and developed the first nuclear power plant (NPP) in the world with gas coolant and a directly closed gas turbine cycle called ML-1 transportable NPP [2]. Simultaneously, another transportable reactor, called the Pamir-630D [2] plant, was

This work was supported by the National Natural Science Foundation of China (No. 12005290), the Chinese TMSR Strategic Pioneer Science and Technology Project (No. XDA02010000), and Youth Innovation Promotion Association of the Chinese Academy of Sciences (No. 2020261).

✉ Gui-Feng Zhu
zhuguifeng@sinap.ac.cn

✉ Yang Zou
zouyang@sinap.ac.cn

[1] Shanghai Institute of Applied Physics, Chinese Academy of Sciences, Shanghai 201800, China

[2] University of Chinese Academy of Sciences, Beijing 100049, China

developed in the Soviet Union. The feasibility of transportable microreactors was confirmed by experiments. However, both were shut down because of incorrect choice of coolant. With the revival of the second nuclear era [3], small reactors again gained attention and began to play an important role in the nuclear industry and transportable microreactors became a key topic in microreactor research as their output power can satisfy the needs of industrial facilities, remote rural areas, and mineral areas that are not connected to a central power grid. The advanced integrated design philosophy of transportable microreactors, which ensures small size, high inherent safety, simplified auxiliary system, and modular transportation, improves their ability for rapid deployment and operation. The request for site installation and maintenance operations is decreasing due to its integrated and high-security design. Coupled with their excellent anti-proliferation performance, transportable microreactors have aroused the interest of developing countries with dispersed populations that cannot afford large nuclear plants.

Table 1 shows some of the different types of small transportable reactors that have been developed in recent years. The most common fuels are pure ceramic fuel, U metal, or coated particle fuel, which is more secure, but with lower fuel loading. Recently developed reactors (Table 1) are mostly heat pipe-, liquid metal-, and gas-cooled conceptual designs. In gas-cooled reactors, the coolant can be directly connected to the power generator, omitting the requirement for a heat exchange device and other auxiliary systems, making them more suitable for miniaturization. Such a similar gas-cooled reactor listed in Table 1 is the micromodular reactor (MMR) [10–12] designed by the Department of Nuclear and Quantum Engineering, Korea Advanced Institute of Science and Technology, which adopts S-CO_2 as a coolant that directly flows into the power conversion system to realize an integrated system. The feasibility of such a design using S-CO_2 was proven by neutronic and thermal–hydraulic simulations. Moreover, analysis in the literature [17] and the first 5 MWe S-CO_2 cycle power generation test unit successfully put into operation with all indicators fully meeting the design requirements have further confirmed the implementability and reliability of the S-CO_2 power cycle at the MW level.

With its vast area and large population, China is the most promising market for transportable microreactors. The objective of this study is to design an integrated long-life S-CO_2 cooled vehicular microreactor (VMR) for remote regions based on tristructural isotropic (TRISO) fuel particles. The VMR should be extremely safe and highly fuel-efficient. The S-CO_2 coolant for the VMR designed in this study is directly connected to the power generation system for power generation. It can be seen from Table 1 that the core life using TRISO fuel particles is shorter than that using other fuels; therefore, a longer life requires a larger core volume, which contradicts the small size requirement. Therefore, the main challenge is that this study is achieving a long life with a small core size while using TRISO particle fuel.

2 Reactor description and design method

2.1 Design principles

VMRs are mainly designed for long-term use in areas far from power grids and can generate 5 and 1–2 MW of

Table 1 Transportable small modular reactor research

Country	Reactor	Power	Size (*R*/*H*)	Fuel	Coolant	Lifetime
USA	ML-1 [2]	3.3 MW	–/0.56 m	–	Nitrogen	–
	Megapower[4]	5 MW	183 cm /366 cm	UO_2	Heat pipe	12-20EFPY
	SSTAR [5]	19.8 MW	61 cm/97.6 cm	$U^{15}N$	Pb	30EFPY
	TFHR [6]	20 MW	1.5 m/1.3 m	$UC_{0.5}O_{1.5}$, TRISO	Flibe	540EFPD
	VSLLIM [7]	1–10 MW	–/1–2 m	UN (13.76%)	Sodium	5.9EFPY
	EVinci^{TM} [8, 9]	0.2 MWe	–	–	Heat pipe	> 10EFPY
	SPR [9]	5 MW	77.85 cm/150 cm	UO_2	Heat pipe	–
Russia	Pamir-630D [2]	4.95 MW	–/0.5 m	–	N_2O_4	1-2EFPY
Korea	MMR [10–12]	36.2 MWe	0.82 m/2.8 m	UN	S-CO_2	20EFPY
Japan	4S-10ML [13]	10 MWe	1.275 m/14 m	U metal	Sodium	30EFPY
Netherlands	U-Battery [14]	20 MW	1.8 m/–	UO_2, TRISO	Helium	4EFPY
China	STLFR [15]	20 MW	78.85 cm/1.35 m	UO_2 (19.75%)	LBE	18EFPY
	LSMR [16]	5 MW	0.5 m/2.8 m	–	LBE	> 10EFPY
	$(MS)^2R$ [17]	1 MWth	0.445 m/0.91 m	LiF-UF_4 (93%)	Heat pipe	> 5EFPY

thermal and electric power, respectively, sufficient to satisfy the demand of remote rural and mineral areas with populations of 10,000–20,000. In this study, to reduce maintenance and achieve a high-security reactor core, the selection of materials, structure, and power generation system for the VMR were set based on several design and optimization principles:

1. The simplified auxiliary system and integrated design, reactor module, and power generation module are connected directly.
2. Small size and compact core design, allowing two modules to be placed into one container with a width and height of less than 2.4 m for transportation.
3. Easy deployment and on-site installation for quick operation after establishing simple shielding measures.
4. Excellent inherent safety and nuclear nonproliferation capability, without high radioactive release under accidents.
5. Long core life, no refueling, and no maintenance with the container returning to the processing plant at the end of its lifetime.
6. Competitive economics, including high fuel efficiency, high neutron economy and low construction and maintenance costs.

Based on these principles, the VMR design should be secure for use in remote areas, with a long-life and high fuel efficient reactor core.

2.2 Thermoelectric conversion module

In this study, the VMR used S-CO_2 as the coolant which was directly connected to the gas turbine to drive the generator for the Brayton cycle. Microreactors generally use gas, liquid metal, or heat pipes as cooling media. Compared with other reactors, heat pipe-cooled reactors have the advantages of easy starting, not requiring high pressure, and high security of the core. However, too many heat pipes complicate the core structure. Liquid metal-cooled reactors are flexible and can be combined with different thermoelectric conversion systems; however, the high chemical activity will corrode the core material. In contrast, gas coolants usually exhibit low activity and can operate at high temperatures with no phase change in gas-cooled reactors. The advantage of gas-cooled reactors is that the gas can be directly connected to the turbine without a heat exchanger, despite its low density and high compressor power [18].

The three most efficient cycles of thermoelectric conversion units are the Stirling, closed Brayton, and Rankine cycles. In the Rankine cycle, a phase change occurs during operation which will be a problem when the coolant gas directly connects to power generation system, while the Stirling and closed Brayton cycles use inert gas as the working medium, avoiding the problem of phase changes. The Stirling conversion system is primarily composed of a Stirling engine, a type of piston engine with external heating that operates in a closed regenerative cycle [19] and is characterized by its high efficiency and long life. However, owing to the output power limitation, the Stirling cycle is only suitable for reactors with power at the kilowatt level. Closed Brayton cycle technology was proposed by NASA in the early 1960. The thermal properties of the Brayton cycle are directly related to the physical properties of the working medium, which is usually helium or a mixture of helium and xenon [20]. The supercritical cycle is another type of Brayton cycle that uses supercritical gas. The most studied working medium for the supercritical cycle is S-CO_2, which is non-toxic, rich in reserves, and economical. Compared with the normal Brayton cycle, the supercritical cycle utilizes the property mutation phenomenon of S-CO_2 in the near-critical region, setting the compressor operating temperature around the near-critical temperature of high density and setting the reactor operating temperature above the critical temperature of low density to decrease the power dissipation of the compressor, solving the problem of high compressor power dissipation and significantly improving the thermoelectric conversion efficiency. In addition, owing to the high pressure and low flow rate in the system, the sizes of the compressor and turbine in the supercritical cycle are several orders of magnitude smaller than those in helium Brayton and water-Rankine cycles with the same power output; therefore, the overall footprint of the power conversion system can be significantly reduced [21–24]. Based on these advantages and the design principles of the VMR in this study, S-CO_2 was selected as the coolant and directly connected to the power generation system for the Brayton cycle to achieve a small-sized and integrated reactor.

2.3 Fuel type

As the core S-CO_2 coolant is directly connected to the turbine, the radioactive material will be brought to the power generation system if the fuel assembly cladding is damaged, leading to radiation leakage, which will severely affect the life of the power generation system and personnel safety of operators and maintainers. Therefore, to ensure long-term and reliable operation and reduce equipment maintenance demands and accident probability, highly secure TRISO fuel particles were used as fuel. As shown in Fig. 1, traditional TRISO [25] particles consist of a fuel kernel and four coating layers: the buffer, inner pyrolytic carbon (IPyC), silicon carbide (SiC), and outer pyrolytic carbon (OPyC) layers, from inside to outside. The buffer layer is primarily used to store the gaseous fission products produced by the kernel. The role of the IPyC layer

is to prevent the release of gas and solid products, alleviate erosion of the SiC layer, and share part of the internal pressure. The compact SiC layer mainly withstands the pressure produced by fission gas and maintains the integrity of the fuel particles. The OPyC layer prevents mechanical damage to the SiC layer from the outside. Therefore, the TRISO fuel configuration effectively contains actinides and fission products within the particle to prevent leakage and contamination of the coolant and to improve firmness and high-temperature resistance, which guarantees the inherent safety of the reactor [26]. Furthermore, the extreme difficulty and high cost of separating fission products from burnt TRISO particles make it highly resistant to nuclear proliferation.

TRISO particles have proven operating experience in high-temperature gas-cooled reactors (HTGR), which generally use carbon-based matrix, such as graphite. To satisfy design principles 1 and 2, TRISO particles and graphite were chosen as the fuel and matrix materials, respectively. The core fuel inventory using TRISO particles is known to be lower than that of ceramic or metal fuels. Therefore, to improve the fuel density in the VMR, $U^{15}N$ was used as fuel, which has a higher U atomic density than UO_2 (most commonly used in TRISO), in TRISO particles with a large kernel radius of 500 μm to increase the fuel volume fraction (VF). The enrichment of ^{15}N is 95% in order to reduce the harmful neutron absorption of ^{14}N. The ^{235}U in $U^{15}N$ was enriched to 20% and all specific parameters are listed in Table 2.

2.4 Fuel assembly

To improve the fuel volume fraction of the VMR core, it was crucial to determine an appropriate fuel assembly structure.

The most common fuel assembly types are spherical, rod, plate, and prism fuels, among which spherical- and prism-type fuel elements are generally used in HTGR. Spherical fuel elements [27] can realize online refueling, but the fuel loading capacity is inferior to that of prismatic fuel elements. In addition, prismatic fuel also has better radial heat dissipation. Based on the characteristics of prismatic fuel elements, to enhance the fissile material loading capability, for the VMR, this study used a prismatic-type tube-in-duct (TID) assembly, which can achieve a higher fuel volume fraction and lower coolant volume fraction than similar pin-type assemblies with the same pitch. The specific structure of the TID module utilized in the VMR consisted of an intermediate fuel segment and 10 cm-thick upper and lower reflectors, as shown in Fig. 1, constructed using the same material as the radial reflector. A hole in the middle of the fuel assembly was used as a coolant channel. The fuel segment was filled with TRISO particles in a graphite matrix and coated with graphite cladding on the outer wall. The specific parameters are summarized in Table 3.

2.5 Reflector

Graphite, MgO, and BeO were evaluated as candidate reflector materials. Graphite is the most used reflector material and thus has an extensive operational history in reactors. MgO has good radiation resistance and high stability, as well as the lowest density among the three candidates, making it easier to transport. BeO is the most effective reflector of the three owing to it having the largest neutron scattering cross section. BeO was selected as the reflector in the VMR based on the results of the neutron performance evaluation, described in detail in Sect. 3.1.

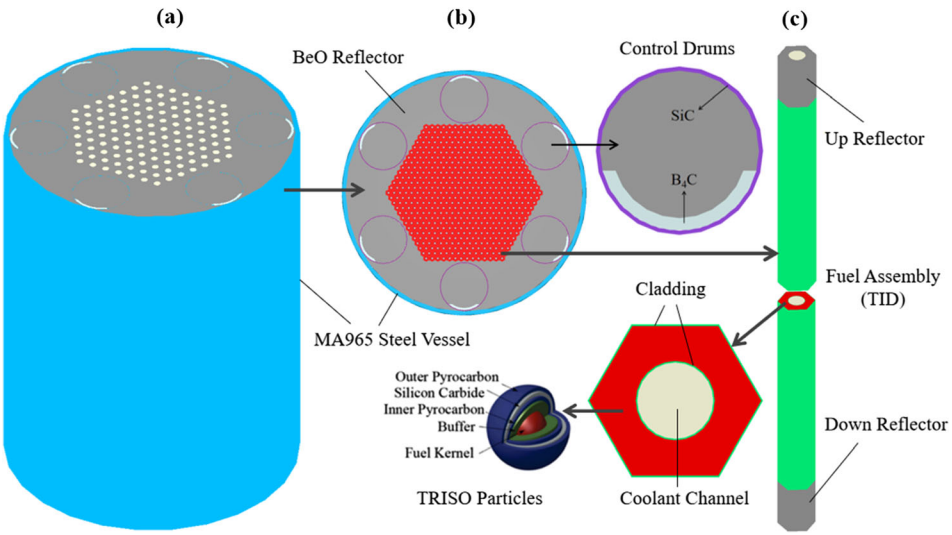

Fig. 1 (Color online) Layout of Vehicular Microreactor: **a** external view, **b** radial cross section view, **c** fuel assembly structure view

Table 2 Parameters of fuel particles

	Materials	Thickness/radius (μm)	Density (g cm^{-3})
Fuel	$U^{15}N$	500	13.4
Matrix	Graphite	–	1.9
TRISO	Buffer	90	1.00
	IPyC	35	1.87
	SiC	35	3.20
	OPyC	35	1.87

Table 3 Parameters of TID fuel assembly

Parameter	Value
Half across flat (cm)	1.5
Height of assembly (cm)	150
Thickness of up/down reflector (cm)	10
Coolant channel radius (cm)	0.45
Thickness of graphite cladding (cm)	0.1

Table 4 Initial main parameters of VMR

Parameter	Value
Power (MWth)	5
Reactor radius/height (cm)	63/154
Thickness of pressure vessel (cm)	2
Reflector outer radius (cm)	61
Cylinder number of assembly	13
Fuel type	TRISO fuel particle
Packing factor	40%
Fuel and enrichment	$U^{15}N$ with 20wt%^{235}U
Coolant	S-CO_2
Inlet/outlet temperature (°C)	410/600
Reactivity control system	Six control drums

2.6 Reactivity control system

To facilitate transportation, the core auxiliary system must be simplified as much as possible. However, the control rod in a microreactor is complicated to operate and has high requirements for the core height, which is not conducive to reducing core size. Therefore, to reduce unnecessary auxiliary systems and operations, a control drum was utilized in the VMR as a control system instead of a control rod, which is easier to operate and can minimize the VMR core height. Rotating the control drum can adjust reactivity by redirecting the neutron absorber for easy operation and can minimize the overall height of the reactor system for transportation. Figure 1 shows the schematic of the control drum. The internal material of the control drum was BeO. The arc-shaped neutron absorber on the drum's surface was B_4C [28]. The outer cladding material was SiC with 0.1 a thickness. Parameters such as the size of the control drum and the thickness of the neutron absorber will be adjusted based on the excess reactivity after determining the final VMR core scheme.

2.7 The preliminary model and parameters of VMR

Figure 1 shows the systematic layout of the preliminary design model of the 5 MW VMR. The radius and height of the reactor vessel were 63 and 154 cm, respectively, and the vessel material was 2-cm-thick MA965 steel. The height of the side reflector and the fuel region inside the reactor vessel was 150 cm, and six control drums were symmetrically embedded in the side reflector. The hexagonal active fuel region with an equivalent half across flat (HAF) of 35.5 cm was surrounded by the reflector layer, consisting of 13 circles of TID fuel assemblies, as shown in Fig. 1. The HAF of the TID assembly was 1.5 cm and the fuel segment inside the graphite cladding was filled with TRISO particles dispersed in a graphite matrix, as described in Sect. 2.4. The packing factor (PF), referring to the proportion of TRISO particles in the region of TRISO particles and graphite matrix, was used to measure the number of TRISO particles in the fuel assembly [29]. In the preliminary VMR model, the PF of the TRISO particles was set to 40%. The other parameters are listed in Table 4.

2.8 Computational methodology

Fluctuations in the design parameters of the VMR affect the reactor core performance. During the optimization process, a series of configurations were analyzed to attain the final core design of the system, which is favorable to the neutronics aspect of the design. In this study, the reflector material was first determined based on the preliminary structure design. The next step was to obtain the optimal design of the VMR. First, keeping the size of the fuel region unchanged, the outer diameter of the reflector, size of the TID assembly, coolant ratio, size of the TRISO fuel kernel, and PF were altered to calculate and analyze the effect of these parameters on the reactivity, neutron spectrum, core life, and depletion. Second, keeping the reactor vessel size of the VMR unchanged, that is, the outer radius of the reflector was fixed at 80 cm, the size of the fuel region was changed by varying the cylinder number of assembly (COA) to calculate and analyze its influence on the reactivity, power distribution, temperature reactivity coefficient (TRC), core life, and depletion. Subsequently, the characteristics of the different core configurations were

compared and analyzed according to the above calculation to obtain the final VMR model. Then, based on the optimal VMR, the parameters of the control drums were determined and some important safety parameters were analyzed. The goal of this design was to reduce the overall size and enhance the neutron economy as much as possible.

The Scale6.1 [30] program was used to simulate different types of reactor models of various configurations and the calculation results were analyzed to determine the ideal VMR parameters. To reduce the standard deviation, the number of neutron source particles in the calculation was more than 2.5 million. The statistical error of k_{eff} was $<$ 0.00006. In all calculations, to restrict the scope, some of the parameters were fixed at the initial design value, except for variables or special explanations. It is worth noting that the control drums were not considered in the process of optimizing the initial model to obtain the best VMR because the position and parameters of the control drum can be affected by the size changes of the reflector and active zone. Thus, the specific parameters of the control drums were finalized after determining the optimal VMR configuration.

3 Neutronic result and analysis

3.1 Materials and thickness of the reflector

This section describes the different effects of three different reflector materials in the core. Figure 2a shows that the curve of core reactivity varies with different reflector outer radii when MgO, graphite, and BeO are used and compares the reactivities of the VMR using CO_2 and helium. The effective multiplication factors (k_{eff}) for CO_2 and helium were almost identical, demonstrating that CO_2 did not cause additional harmful absorption to neutrons. Otherwise, the reactivity of the core using BeO as a reflector was much higher than that of MgO and graphite owing to its large neutron elastic scattering cross section and small absorption cross section. Consequently, the outer radius of the BeO reflector was far smaller than that of the graphite and MgO reflectors when k_{eff} was identical. Therefore, from the perspective of reducing the core size, the BeO reflector was more suitable and was thus utilized to obtain the best neutron property in the VMR core. Additionally, it is obvious that k_{eff} increased steadily with an increase in the outer radius of the BeO reflector and tended to be stable when it reached a certain value. The dominant factor for this phenomenon is that when the reflector volume increased, the fraction of core equivalent neutron leakage (absorbed by the reflector and escaping from the core) decreased and the neutron utilization coefficient of the fuel increased owing to the enhanced reflection ability, as depicted in Fig. 2b. Figure 2c shows the neutron spectrum for different BeO outer radii. The neutron spectrum became softer with increasing reflector thickness because some neutrons were moderated in BeO before re-entering the fuel zone.

Similar to the law of reactivity, both the core lifetime and burnup grew with increasing reflector size because of the increased neutron utilization efficiency in the core; however, this growth was in a manner of gradually reducing sensitivity, as shown in Fig. 3. Therefore, it can be summarized that the larger the reflector size, the better the core neutron performance. However, this trend gradually levels off as the reflector outer radius exceeds 80 cm, meaning that a continuous increase in the reflector size will not improve the neutron economy while hindering core miniaturization. Based on the above analysis, and the fact that the lifetime and burnup of the core with an 80 cm reflector outer radius were almost twice that at 60 cm, the radius of the reflector will be amplified from 61 to 80 cm in the following research for better neutron performance.

3.2 Size of fuel assembly and the coolant ratio

To understand the influence of the coolant ratio and fuel assembly size on the reactor neutron performance, the k_{eff} of different assembly HAF was calculated when the coolant ratios were 10%, 20%, and 30%, under unchanging reactor fuel region conditions.

The results shown in Fig. 4a illustrate that k_{eff} increased with the enlargement of assembly HAF and reduction in coolant ratio and showed greater sensitivity to fluctuations in the coolant ratio than in assembly size. This is because a reduction in the coolant ratio can significantly enhance the fuel loading in the core, thereby increasing the reactivity. However, when the component size increases, the proportion of cladding in the fuel assembly will slightly decrease, significantly increasing the fuel loading. In addition, the expanded lattice distance will lead to an increase in the resonance escape probability of neutrons because of the space self-shielding effect between assemblies. Thus, both effects result in reactivity with a small increasing trend. Another characterization performed was the neutron spectrum, shown in Fig. 4b, c. Changes in both the coolant ratio and assembly size affected the neutron energy distribution but the former had a more pronounced effect.

Considering the neutron performance in the VMR, the coolant ratio was determined to be 10% as a priority because of its high sensitivity. The assembly size, which has little effect on k_{eff}, can deteriorate the heat transfer in the VMR core. Therefore, from the perspective of neutronics and heat transfer, the assembly HAF was set at an initial design value of 1.5 cm and the coolant channel radius was adjusted to 0.498 cm, as depicted in Fig. 5.

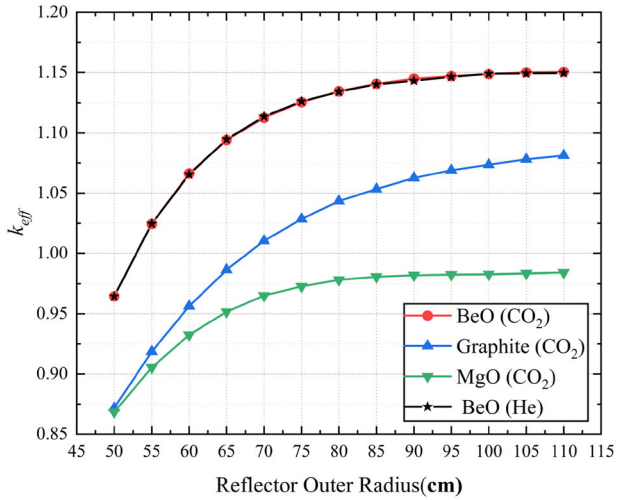

(a)

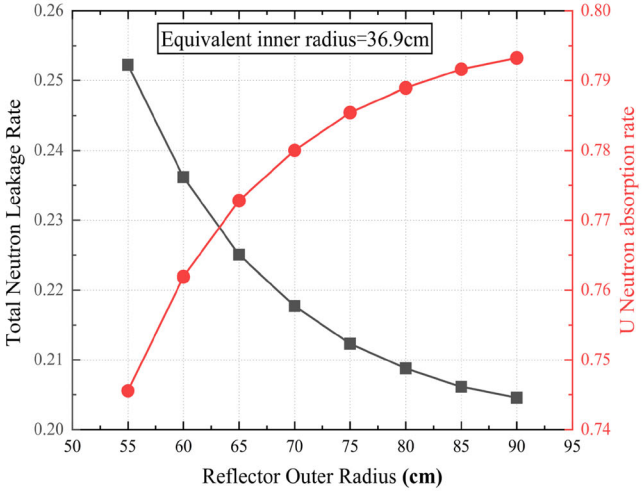

(b)

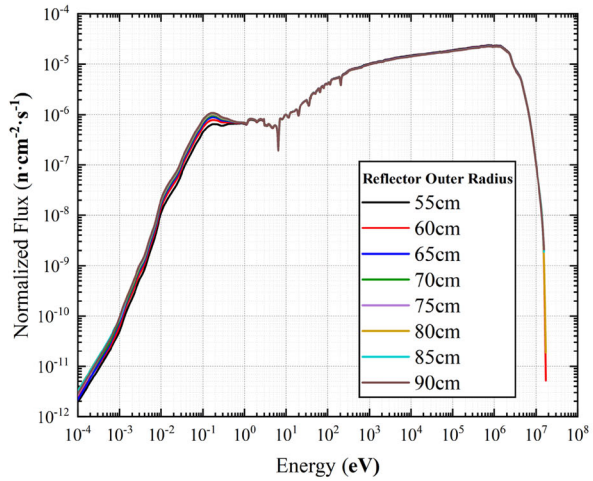

(c)

Fig. 2 (Color online) **a** k_{eff} curves under different models of reflector outer radius with different reflector and coolant material. **b** The ratio of neutron escaped and absorbed by U under different models of BeO reflector outer radius. **c** Neutron spectrum in active core under different models of BeO reflector outer radius

3.3 Size of TRISO kernel and the packing factor

Other crucial parameters affecting the core properties are the kernel radius and PF of TRISO particles, the values of which were 500 μm and 40%, respectively, in the initial design model. In this section, without changing the thickness of the coating layer of the TRISO, the influence of PF increasing from 10 to 40% on k_{eff} was calculated when the kernel radius increased from 100 to 500 μm. In addition, changing the TRISO kernel size and PF is equivalent to changing the fuel inventory in the core. The calculation results are shown in Fig. 6a, with the $U^{15}N$ inventory of the reactor core having different PF and kernel radii as the *X*-axis coordinate and k_{eff} as the Y-coordinate. Each curve represents the results of the core model with PF values of 10%, 15%, 20%, 25%, 30%, 35%, and 40% with the kernel radius fixed. k_{eff} on the curve with a kernel radius of 100 μm has a maximum value and shows a trend of first increasing and then decreasing. This phenomenon results from the fact that the C/U ratio in the VMR core decreased with an increase in both the kernel size and PF of TRISO. The VMR core with a small PF of 10% had a large C/U ratio, was over-moderated, and then transitioned to an under-moderated state along with a lessening C/U ratio caused by increased PF, which was responsible for the k_{eff} rising to a maximum and then falling. When the kernel radius increased to 150 μm, the k_{eff} curve monotonically decreased. When the kernel radius was 200 μm, the k_{eff} curve still showed a downward trend, but the slope of the curve gradually diminished. This is because even if the PF

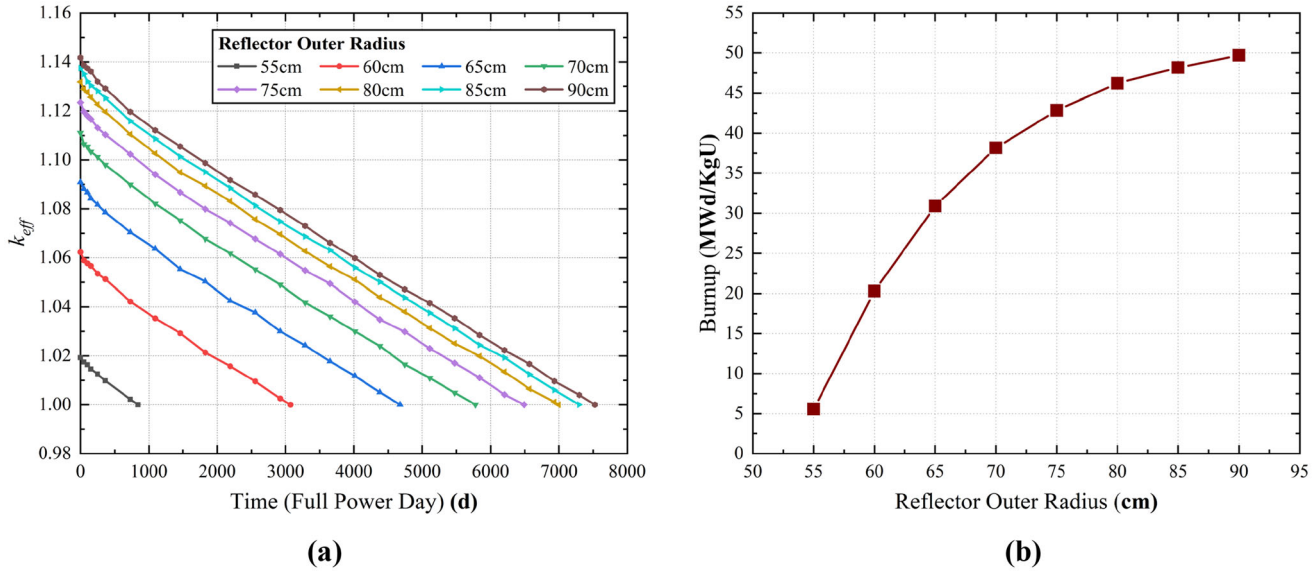

Fig. 3 (Color online) **a** k_{eff} curves with time under different models of BeO reflector outer radius. **b** Burnup under different models of BeO reflector outer radius

is 10%, the C/U ratio is already so small that the VMR core is in an under-moderated state. Therefore, these two k_{eff} curves decreased with increasing PF. However, as the kernel radius increased to 250, 300, 350, 400, 450, and 500 μm, k_{eff} increased progressively, following a small decrease. The larger the kernel radius, the larger the k_{eff} value and the earlier the inflection point. This is due to the resonance absorption effect of U in the resonance region. In the under-moderated state, as the C/U ratio decreases, the core neutron spectrum becomes increasingly harder, leading to an increase in the neutron capture probability. When the neutron spectrum occurs in the resonance region of U, the core has the lowest neutron utilization and k_{eff} is minimal. Subsequently, as the energy spectrum continues to harden with further carbon reduction, the resonance absorption effect gradually weakens, and the fission caused by fast neutrons gradually increases. Therefore, the k_{eff} curves of kernel radius larger than 250 μm increase after the minimum instead of continuing to decrease. In summary, with the increase in fuel inventory, k_{eff} first increases, then decreases, and then continually increases after reaching the minimum value.

Based on the above analysis, the influence of fuel inventory on the core lifetime and burnup was explored for fuel inventories of 602 (r_{kernel} = 500 μm, PF = 30%), 641 (r_{kernel} = 450 μm, PF = 35%), 655 (r_{kernel} = 400 μm, PF = 40%), 702 (r_{kernel} = 500 μm, PF = 35%), 732 (r_{kernel} = 450 μm, PF = 40%), and 803 kg (r_{kernel} = 500 μm, PF = 40%). The results demonstrated that a higher fuel inventory leads to a harder neutron spectrum and a larger core lifetime and burnup, as shown in Fig. 6b, c. It is worth emphasizing that the reactor core will exhibit similar characteristics providing the total fuel inventory is the same, even if the kernel size and PF differ.

The difficulty of the fabrication process for matrix dispersion fuel assembly increases with increasing TRISO PF, with the maximum PF that can be achieved being 40%. In contrast, it is easier to enhance fuel inventory by augmenting the fuel kernel size rather than increasing PF. However, the heat transfer ability of TRISO particles can deteriorate with an excessively large kernel size. Therefore, the maximum kernel radius of the TRISO particles adopted in the VMR was 500 μm and the PF was determined to be 40%.

3.4 Size optimization analysis of active core

Based on the above analysis, the HAF of the TID assembly, coolant ratio, TRISO kernel radius, and PF were determined. For the active core, the volumes of the fuel and reflector need to be adjusted to find the optimal $V_{\text{fuel}}/V_{\text{ref}}$ that gives the VMR core the best neutron economy and highest fuel efficiency. Therefore, the reflector outer radius was fixed at 80 cm and the proportion of $V_{\text{fuel}}/V_{\text{ref}}$ was altered by varying the COA from 10 to 17 in the active core to study the changing rule of reactivity, power distribution, neutron spectrum, depletion, and TRC. The simulation model is shown in Fig. 7.

Figure 8a shows the calculation results for k_{eff}. When the reactor volume was fixed and the active region expanded, the effective thickness of the reflector decreased, causing neutron leakage from the core to increase and reducing harmful absorption by BeO. However, the total neutron loss proportion summing these two effects

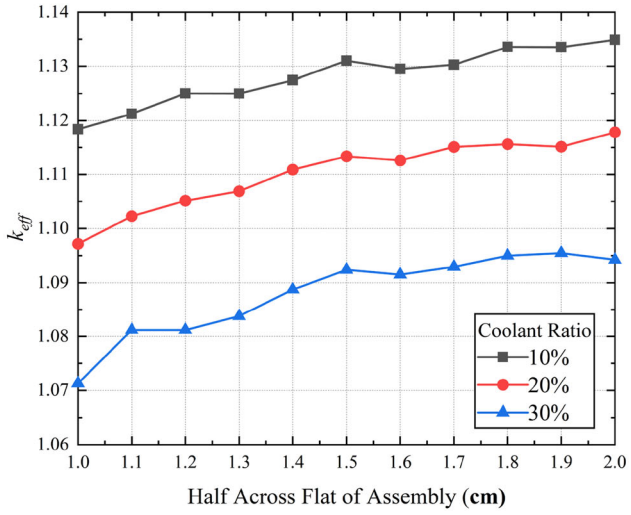

(a)

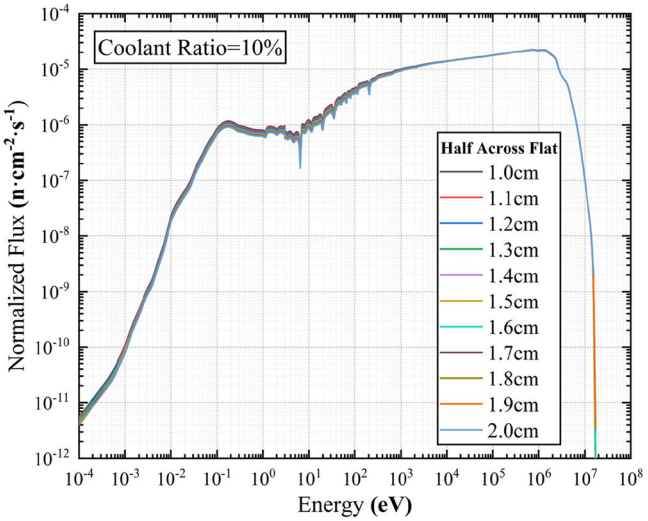

(b)

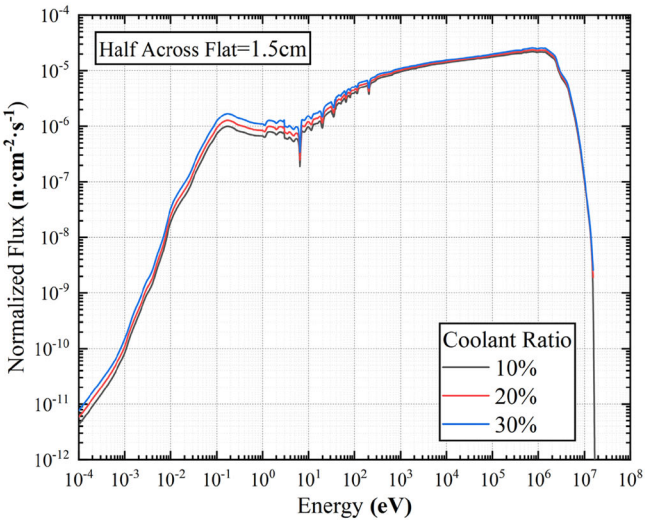

(c)

Fig. 4 (Color online) **a** k_{eff} curves under different models of assembly half across flat with different coolant ratios, when the outer radius of BeO reflector is 80 cm. **b** Neutron spectrum under different models of assembly half across flat, when coolant ratio is 10%. **c** Neutron spectrum under different models of coolant ratio when assembly half across flat is 1.5 cm

generally decreased, as shown in Fig. 8b, leading to higher reactivity in the core. The reduction in the reflector volume can lead to core neutron spectrum hardening, improving the resonance absorption of fast neutrons by the fuel, as shown in Fig. 8b, resulting in a smaller resonance escape probability and thus leading to a decrease in k_{eff}. Therefore, these two decisive factors interact to make k_{eff} exhibit the characteristic of growing first and then dropping. The COA corresponding to the maximum value was 13.

Figure 8c presents the power distribution results of the fuel assemblies on the diagonal of the core. Taking a core with a COA of 14 as an example, Fig. 8d shows the two-dimensional power distribution profile. The power density

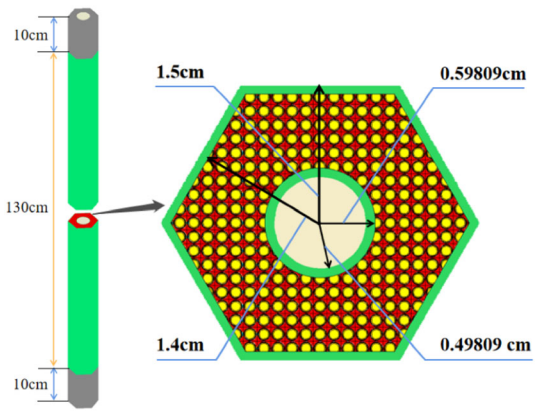

Fig. 5 (Color online) Finalized TID fuel assembly and its parameters

of fuel assembly in the periphery was higher than that in the center for all eight simulation models. The power density of the six apex angles was obviously higher than that in the other assemblies in Fig. 8d, which results in a sharp increase in the power density in the outermost assembly, as shown in Fig. 8c. This can be attributed to the fact that the BeO reflector has excellent reflection ability and good moderating ability for neutrons. Most of the neutrons leaking from the active zone may slow and re-enter the fuel. This leads to a significant increase in the thermal neutron flux in the fuel assembly at the edge of active core, distorting the power density distribution. As the COA increased from 10 to 17, it can be observed from Fig. 8c that the overall core power density decreased gradually but the sudden increase in edge power density did not change significantly with the expansion of the active region. That is, from the perspective of power distribution alone, there was no obvious advantage for any model. However, from the perspective of thermal hydraulics, the power distortion behavior will damage the structure of the fuel if the core temperature is too high. In this respect, a larger active core is more reliable, because the power density decreases with the increase in the active core size, as can be seen from Fig. 8c, so does the core temperature. In fact, even for the core with a COA of 10, the power density in the periphery did not exceed 50 MW/m^3,

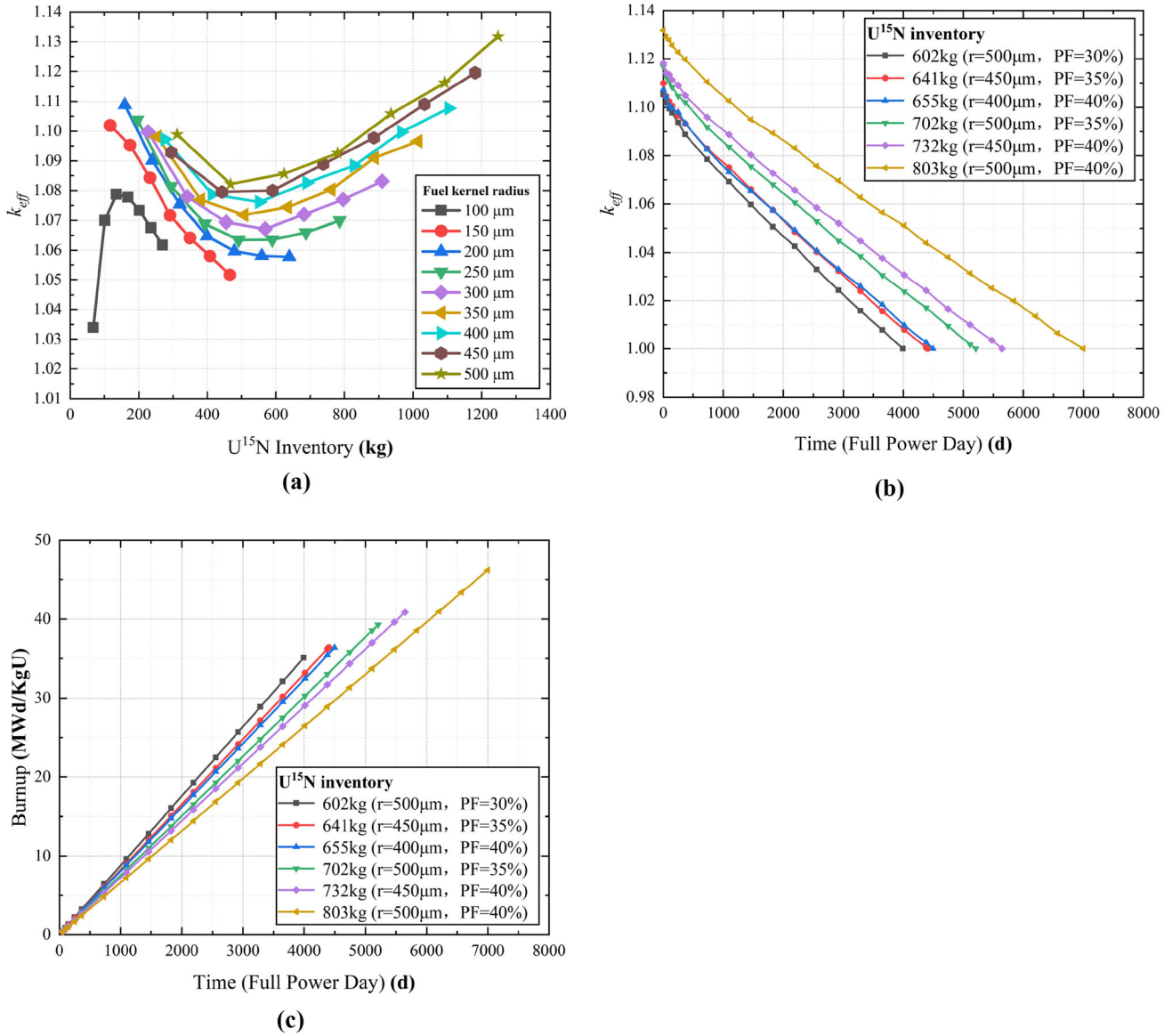

Fig. 6 (Color online) **a** k_{eff} curves with U^{15}N inventory of the reactor core with different PF and kernel radius as *X*-axis coordinate. When the kernel radius is fixed, each single curve represents the results of the core model with PF values of 10%, 15%, 20%, 25%, 30%, 35%, and 40%. **b** k_{eff} curves with time under different models of fuel inventory. **c** Burnup under different models of fuel inventory

which is a relatively small value. However, to prevent it from deteriorating the heat transfer in the fuel assembly and destroying the fuel structure, it is preferable to improve this phenomenon.

The results of depletion under different COAs are shown in Fig. 9 a, b. Unsurprisingly, the core lifetime increases almost linearly with the increase in COA because expanding the fuel area enhances the fuel loading capacity and results in a hardened neutron spectrum in the core. As for burnup, the results show a slight upward trend and then a decrease. Evidently, the consumption of ^{235}U will increase with the prolonging of the core lifetime. However, the increase in fuel inventory that causes power density diminution in the reactor core can result in declining ^{235}U utilization and the hardening of the neutron spectrum also causes the proportion of fission reactions caused by ^{238}U to gradually increase. Therefore, because of the simultaneous influence of both of these factors, instead of linearly increasing, the burnup tends to increase to the maximum and then decrease with increasing COA. Maximum burnup occurred in the configuration with a COA of 13. If the fuel zone is expanded, the burnup is expected to decrease dramatically owing to the massive neutron leakage. Therefore, it can be concluded that, in terms of fuel efficiency, the core with a COA of 13, when the overall radius of the reflector was set to 80 cm, was the best VMR configuration, achieving a maximum value of burnup of 46.2 MWd/kgU. However, the core lifetime and burnup of the VMR showed opposite trends when the COA was greater than 13, meaning that, to achieve a long-life core, the high fuel efficiency design requirements may need to be abandoned.

In order to ensure the safe operation of the reactor, the core is required to have negative reactivity effect for reducing core reactivity in the case of a sudden temperature increase, so as to prevent the occurrence of accident. Hence, a negative temperature coefficient is an important parameter for reactor safety. Figure 9c shows the TRC evaluation results. The TRC for all eight cases was negative and showed downward trends with increasing COA. Thus, the higher the COA, the higher the inherent safety in the core.

Based on the above analysis and only considering neutron physics, the VMR core with a COA of 14 is the ideal design, achieving a satisfactory neutron economy with a core life of 7980 days ($\approx$ 21.8 years) and a burnup of 45.7 MWd/kgU, which is only slightly less than the maximum value when COA is 13. In this VMR configuration, the core possesses a relatively flat power distribution and a large negative TRC and the equivalent HAF of the hexagonal fuel zone is approximately 38 cm.

3.5 Physical characteristics analysis based on the optimal VMR

3.5.1 Power optimization for the apex position

Based on the above analysis, the model with a COA of 14 in the active core was determined as the optimal VMR configuration. According to Fig. 8d and the analysis in Sect. 3.4, the power density in the outermost circle of the hexagonal active core was greater than that in the center, particularly for six fuel assemblies at the apex angles, which was the main cause of severe power distortion. This behavior can be improved by partitioning the fuel assembly with different ^{235}U enrichments; however, this can affect fuel burnup, which is a key design criterion mentioned in Sect. 2.1 and will affect the economic competitiveness of VMR. Therefore, to balance the core power distribution and fuel efficiency, only the ^{235}U enrichment of the six assemblies at apex angles was reduced from 20 to 11%. The cross section of the optimized core is shown in Fig. 10a. In this way, the power density of the apex position can be reduced without the loss of a large burnup depth. Figure 10b shows the two-dimensional power distribution profile of the optimized VMR. Compared with the result in Fig. 8d, the optimized apex power density decreased from 26.7 to 19 MW/m^3, which means an effective improvement. Thus, the optimized VMR model shown in Fig. 10a is considered the final configuration of the VMR and other important parameters will be investigated in future studies.

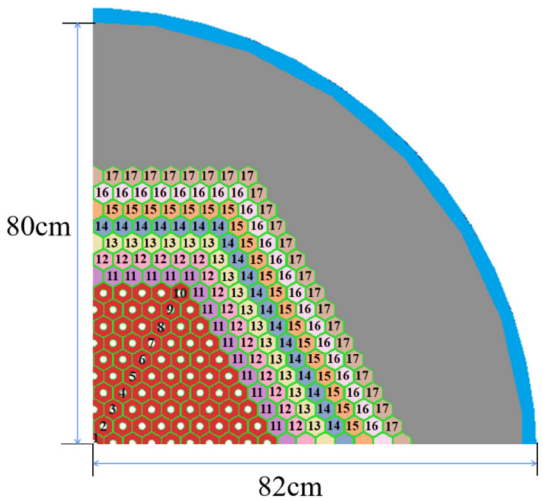

Fig. 7 (Color online) The simulation model of VMR with different COA in the active core when the reactor size is fixed

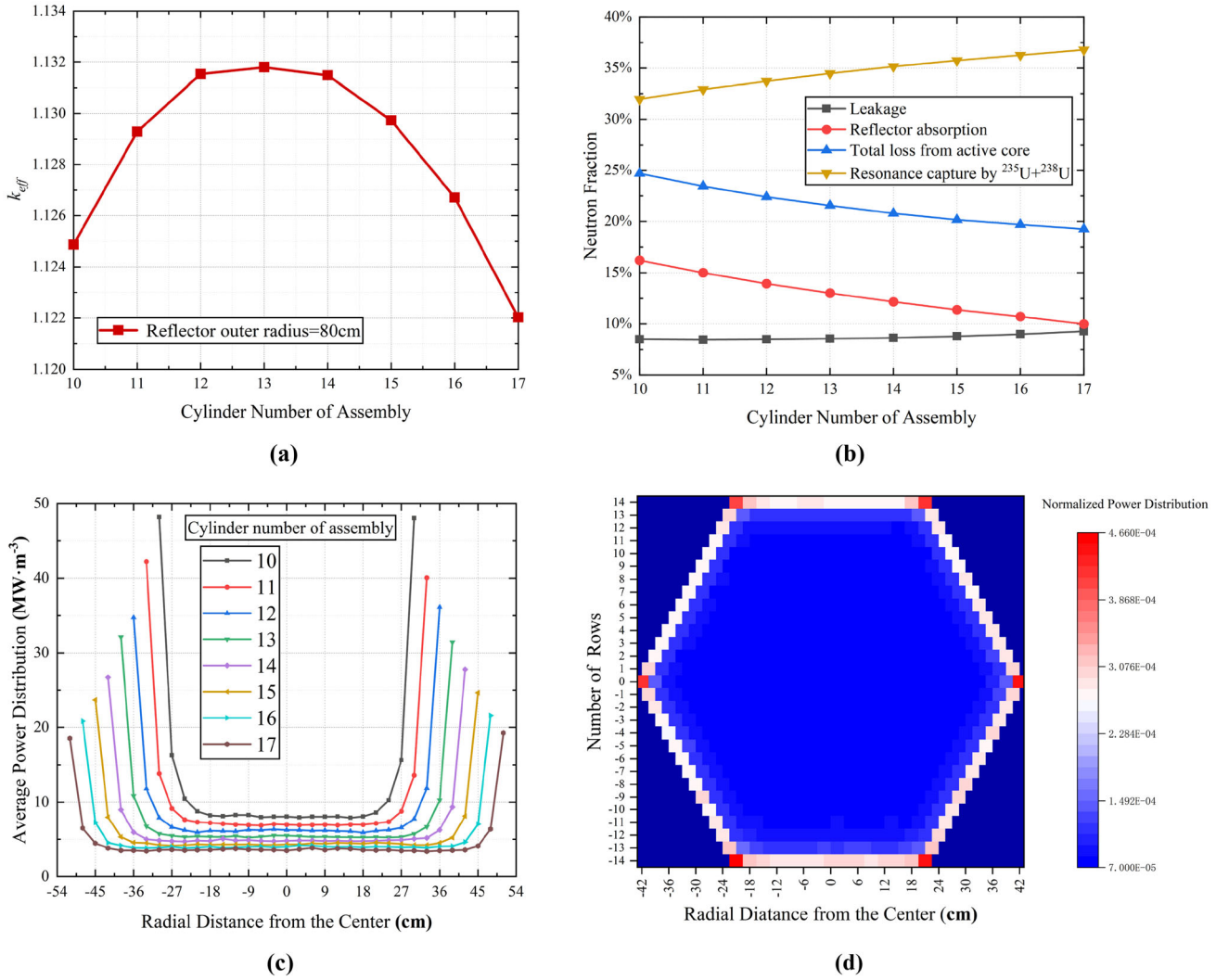

Fig. 8 (Color online) **a** k_{eff} values. **b** Neutron loss in the core under different models of assembly cylinder number. **c** Radial power distribution under different models of assembly cylinder number, when the outer radius of the reflector is fixed at 80 cm. **d** Two-dimensional power distribution profile when COA is 14

3.5.2 Control drum worth

The next step was to determine the parameters of the control drum based on this configuration. First, the overall radius of the control drum was assumed to be 16 cm with 0.1 cm of SiC cladding thickness and 0.5 cm of thickness for the B_4C neutron absorption ring with a radian of 90, as shown in Fig. 11a. The B_4C used was naturally enriched. Figure 11b, c shows the sectional views of the core with all control drums turned to the outside and inside, respectively. The performance of the designed control drums must be assessed to meet safety requirements. Therefore, the reactivity of the core was calculated when the control drums in the VMR core were in the states of Fig. 11b, c and the results of k_{eff} were 1.12392 and 0.97826, respectively, as shown in Table 5. The total worth of the six control drums was 14,566 pcm. These results prove that this type of control drum design guarantees a VMR with a sufficient shutdown margin (2174 pcm), ensuring that the reactor core is sufficiently secure and can respond quickly to reactivity accidents.

3.5.3 Burnup calculation

The core neutron physics properties may be affected by the control drums. Table 6 compares the burnup calculation results of the optimized VMR models with control drums facing outside, as shown in Fig. 11b, and without control drums. The latter can be obtained directly from Sect. 3.4. Because of the existence of control drums, the core life and burnup were slightly reduced to 21 years (7675 days) and

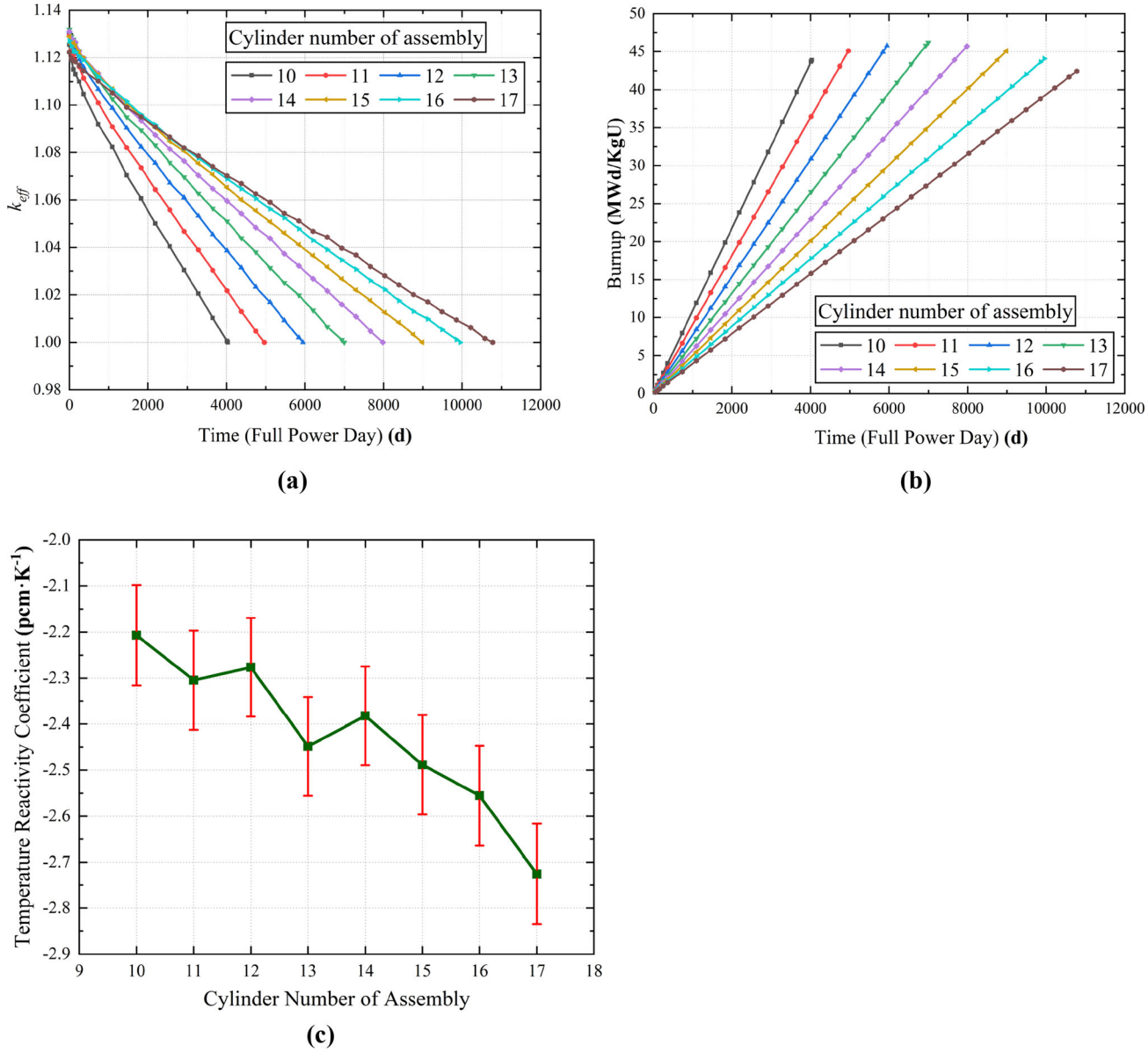

Fig. 9 (Color online) **a** k_{eff} curves with time under different models of assembly cylinder number. **b** Burnup under different models of assembly cylinder number, when the outer radius of the reflector is fixed at 80 cm. **c** Reactivity temperature coefficient under different models of assembly cylinder number, when the outer radius of the reflector is fixed at 80 cm

43.9 MWd/kgU but still met the design criteria of long life and high fuel efficiency.

3.5.4 Reactivity coefficient

The change in the core reactivity caused by the core temperature is called the temperature effect. To ensure safe operation, the reactor core must exhibit a negative reactivity effect. In this section, the reactivity coefficients are calculated, including the total TRC, fuel temperature coefficient (FTC), moderator (SiC and C) temperature coefficient (MTC), and coolant void reactivity (CVR). All the reactivity coefficient results were negative, as shown in Table 7, which means when the core temperature fluctuates, the negative feedback effect will induce an opposite change in power density, allowing the reactor to reach a new steady state. The values of CVR and MTC were less negative than that of FTC and may become positive during VMR operation. However, owing to the large negative value of FTC, the VMR core still had a large negative TRC overall, ensuring the safety of the reactor.

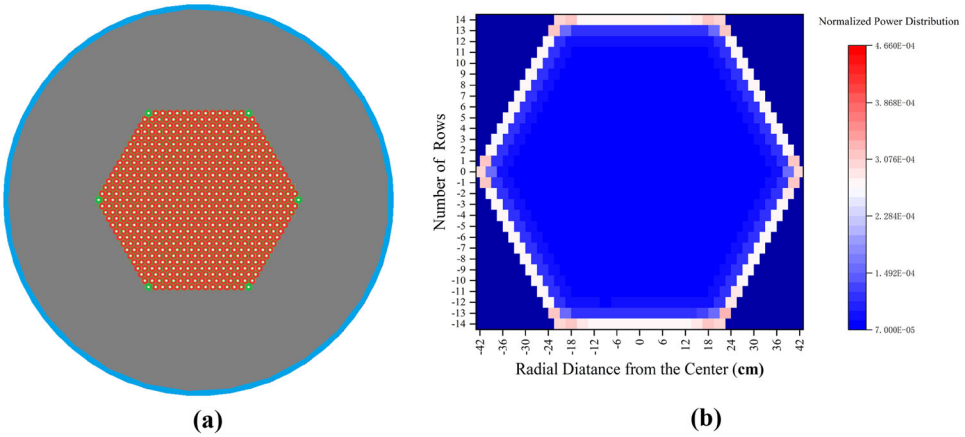

Fig. 10 (Color online) **a** Section view of the optimized VMR when the enrichment of ^{235}U in the fuel assembly at apex angle is 11%. **b** Two-dimensional power distribution profile of the optimized VMR when the enrichment of ^{235}U in the fuel assembly at the apex angle is 11%

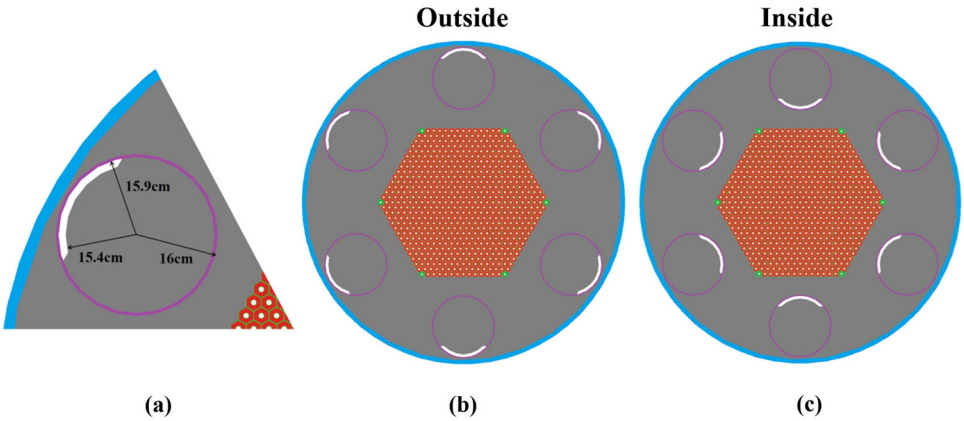

Fig. 11 (Color online) **a** Parameters of control drums, **b** section view of optimized VMR core with control drums turning to outside, **c** section view of optimized VMR core with control drums turning to inside

Table 5 k_{eff} of the optimized VMR with control drums turning to inside and outside

	Outside	Inside	Control drum worth
k_{eff}	1.12392	0.97826	14,566 pcm

Table 6 Burnup results for the optimized VMR with and without control drums

Optimized VMR	Lifetime (years)	Burnup (MWd/kgU)
Without control drums	≈ 21.8	45.7
With control drums	≈ 21	43.9

Table 7 Reactivity coefficient of optimized VMR

Parameters	Value
MTC (pcm/K)	− 0.183
FTC (pcm/K)	− 2.31
TRC (pcm/K)	− 2.63
CVR (pcm)	− 17

3.5.5 Dynamic parameters

The delayed neutron effect cannot be ignored in studies of transient processes and reactor safety control and reactor control takes advantage of the presence of delayed neutrons. Therefore, effective delayed neutron fraction (β_{eff}) is a crucial parameter for studying the dynamic characteristics of reactors. After obtaining the optimized core design configuration of the VMR, β_{eff} and neutron generation time in the VMR core were calculated, achieving values of 0.00706 ± 0.00043 and $(1.7692 \pm 0.0267) \times 10^{-4}$ s, respectively, which are close to the values of the pressurized water reactor [31]. This implies that the VMR is not a very fast reactor, even though its neutron spectrum is harder than that of a thermal reactor.

4 Conclusion

In this paper, an integrated S-CO_2 cooled vehicular microreactor with a thermal power of 5 MW was described. Large TRISO particles and TID fuel assemblies were used in the preliminary core design. The CO_2 coolant was directly connected to the turbine for Brayton cycle power

Table 8 Optimized parameters of the VMR

Parameter	Value
Power (MWth)	5
Reactor radius/height (cm)	82/154
Thickness of reactor pressure vessel (cm)	2
Reflector outer radius (cm)	80
Reflector materials	BeO
Equivalent half across flat of core (cm)	38
Cylinder number of assembly	14
Fuel type	TRISO fuel particle
Packing factor	40%
Fuel	$U^{15}N$
Enrichment	20wt% ^{235}U, 11wt% ^{235}U (apex)
Type of fuel assembly	TID
Half across flat of assembly (cm)	1.5
Radius of coolant channel (cm)	0.498
Materials/thickness of assembly cladding (cm)	Graphite/0.1
Coolant	S-CO_2
Inlet/outlet temperature (°C)	410/600
Reactivity control system	Six control drums
Radius of control drum (cm)	16 cm
Materials/thickness of control drum cladding (cm)	SiC/0.1
Neutron absorber/thickness (cm)	Natural B_4C/0.5

generation to achieve an integrated design and reduce auxiliary systems, and CO_2 was proven to be as transparent as helium to core neutrons. Compared to graphite and MgO reflector materials, the BeO reflector allowed the VMR core to be much smaller, softened the neutron spectrum, and enhanced the core performance. The best reflector outer radius was determined to be 80 cm.

To increase fuel loading and achieve a compact VMR core, parameters such as fuel assembly size, coolant ratio, TRISO particle size, PF, and reflector radius were altered to evaluate and analyze their influence on k_{eff}, neutron spectrum, core life, and burnup. The TID fuel assembly had a remarkable fuel loading capability. The core property showed greater sensitivity to fluctuations in the coolant ratio than in the assembly size. Therefore, the reasonable TID assembly HAF and coolant ratio were set to be 1.5 cm and 10%, respectively. For TRISO particles, an increase in the fuel kernel size and packing factor can significantly enhance the fuel inventory in the core; thus, the core lifetime and burnup increased. Finally, to study the effect of core activity size on core performance, the $V_{\text{fuel}}/V_{\text{ref}}$ was adjusted by changing the number of fuel assemblies in the active zone. The results demonstrated that the lifetime tended to increase progressively when $V_{\text{fuel}}/V_{\text{ref}}$ increased, but the burnup results peaked. Considering all factors, including the power distribution and TRC, the VMR core configuration with a COA of 14 was regarded as the optimal design.

Based on the optimal VMR, the power density of the apex position was optimized by decreasing ^{235}U enrichment. Then, the ideal control drum radius and thickness of B_4C were determined to be 16 cm and 0.5 cm, respectively, which can ensure a fairly deep shutdown margin and the high security of the VMR. The core life and burnup of the optimized VMR with control drums were 21 years and 43.9 MWd/kgU, respectively. Compared to the previous microreactor concepts, as listed in Table 1, the developed VMR with the core fueled by low-enriched TRISO fuel particles better achieved the goals of long life and high burnup. Finally, the reactivity coefficient and dynamic parameters were evaluated and the results proved the inherent safety of the VMR. The complete parameters of the optimized VMR are summarized in Table 8.

The final VMR core configuration obtained in this paper is changeable and can be adjusted based on different demands. However, there are still many details that require further study that will further improve the core fuel efficiency and achieve better radial power distribution.

Author contributions All authors contributed to the study conception and design. Data collection and analysis were performed by Fang-Yuan Zhang and Gui-Feng Zhu. All authors participated in discussions about the data analysis and provided meaningful suggestions. The first draft of the manuscript was written by Fang-Yuan Zhang. Gui-Feng Zhu and Yang Zou guided the study preparation and were in charge of polishing and revising the manuscript.

All authors commented on previous versions of the manuscript. All authors read and approved the final manuscript.

References

1. C.K. Jo, Core nuclear design of a micro modular high temperature gas-cooled reactor, in *Transactions of the Korean Nuclear Society Autumn Meeting*, Yeosu, Korea, pp. 25–26 (2018).
2. M.E. Ganin, V.F. Golovko, N.G. Kodochigov et al., Transportable NPP with open and closed gas-turbine cycle. At. Energy **124**(5), 292–301 (2018). https://doi.org/10.1007/s10512-018-0413-6
3. D.T. Ingersoll, Deliberately small reactors and the second nuclear era. Prog. Nucl. Energ. **51**(4–5), 589–603 (2009)
4. P.R. McClure, D.D. Dixon, D.I. Poston et al., Mobile heat pipe cooled fast reactor system. U.S. Patent 10,643,756, 5, May, 2020.
5. C.F. Smith, W.G. Halsey, N.W. Brown et al., SSTAR: the US lead-cooled fast reactor (LFR). J. Nucl. Mater. **376**(3), 255–259 (2008). https://doi.org/10.1016/j.jnucmat.2008.02.049
6. K. Sun, L.W. Hu, C. Forsberg, Neutronic design features of a transportable fluoride-salt-cooled high-temperature reactor. J. Nucl. Eng. Radiat. Sci. **2**, 031003 (2016). https://doi.org/10.1115/1.4032873
7. M.S. El-Genk, L.M. Palomino, A walk-away safe, very-small, long-life, modular (VSLLIM) reactor for portable and stationary power. Ann. Nucl. Energ. **129**, 181–198 (2019). https://doi.org/10.1016/j.anucene.2019.01.025
8. M.M. Swartz, W.A. Byers, J. Lojek et al., Westinghouse eVinci^{TM} heat pipe micro reactor technology development, in *International Conference on Nuclear Engineering. ICONE28-67519*, V001T04A018 (2021). https://doi.org/10.1115/ICONE28-67519
9. R. Hernandez, M. Todosow, N.R. Brown, Micro heat pipe nuclear reactor concepts: analysis of fuel cycle performance and environmental impacts. Ann. Nucl. Energy **126**, 419–426 (2019). https://doi.org/10.1016/j.anucene.2018.11.050
10. J. Lee, S.K. Cho, S.G. Kim et al., Preliminary S-CO_2 compressor design for micro modular reactor, in *Transactions of the Korean Nuclear Society Spring Meeting*, Jeju, Korea, pp. 12–13 (2016).
11. S.G. Kim, B. Oh, S.J. Baik et al., Conceptual system design of a supercritical CO_2 cooled micro modular reactor, in *Proceedings of ICAPP*, pp. 3–6 (2015)
12. Y. Kim, D. Hartanto, H. Yu, Neutronics optimization and characterization of a long-life SCO_2-cooled micro modular reactor. Int. J. Energy Res. **41**(7), 976–984 (2017). https://doi.org/10.1002/er.3686
13. N. Ueda, I. Kinoshita, A. Minato et al., Sodium cooled small fast long-life reactor "4S". Prog. Nucl. Energy **47**(1–4), 222–230 (2005). https://doi.org/10.1016/j.pnucene.2005.05.022
14. D. Ming, K.J. Leen, Feasibility neutronic design for the reactor core configurations of a 5 MWth transportable block-type HTR. Nucl. Sci. Tech. **24**(4), 040602 (2013). https://doi.org/10.13538/j.1001-8042/nst.2013.04.014
15. C. Lei, H.C. Wu, L.Z. Cao et al., Core design study of Small transportable long-life lead-bismuth cooled fast reactor. At. Energy Sci. Technol. **53**(08), 1451–1458 (2019). https://doi.org/10.7538/yzk.2018.youxian.0778 (**in Chinese**)
16. Z. Chen, Z. Lv, Z.J. Zhao et al., Core optimization of 5 MWth Lead-bismuth cooled Super small Module Reactor (LSMR) based on separative work. Ann. Nucl. Energy **120**, 735–741 (2018). https://doi.org/10.1016/j.anucene.2018.06.030
17. G. Hu, D.Y. Cui, X.X. Li et al., Core preliminary neutronics design of a martian surface molten salt reactor with 1 MWth. Nucl. Tech. **44**, 120603 (2021). https://doi.org/10.11889/j.0253-3219.2021.hjs.44.120603
18. H.H. Mao, D. Zhang, C.T. Gao et al., Study of initial events and safety criteria for CO2 cooled reactor. Nucl. Tech. **43**(6), 060004 (2020). https://doi.org/10.11889/j.0253-3219.2020.hjs.43.060004 (**in Chinese**)
19. M. Zhang, X.D. Cai, Q. Du et al., Research on nuclear reactor in space application. Spacecr. Eng. **22**(06), 119–126 (2013). https://doi.org/10.3969/j.issn.1673-8748.2013.06.021 (**in Chinese**)
20. S.M. Zhou, H.X. Wu, C. Xiao et al., Technology review of free piston sterling linear generator system. Micromotors **46**, 12 (2013). https://doi.org/10.15934/j.cnki.micromotors.2013.12.003
21. Z.X. Zhang, L.L. Wu, Supercritical carbon dioxide Brayton cycle for sodium cooled fast reactor. Silicon Valley **10**, 192–193 (2014). https://doi.org/10.3969/j.issn.1671-7597.2014.10.133
22. Y. Li, Z.Y. Zhang, Prospects of power conversion technology of direct-cycle helium gas turbine for MHTGR. Nucl. Power Eng. **20**(2), 159–164 (1999) **(in Chinese)**
23. J.D. Wang, Y. Feng, D.J. Han, Review on supercritical carbon dioxide power cycle application in sodium cooled fast reactor. Nucl. Sci. Eng. **39**(02), 289–297 (2019). https://doi.org/10.3969/j.issn.0258-0918.2019.02.017 (**in Chinese**)
24. Y.P. Huang, J.F. Wang, Applications of supercritical carbon dioxide in nuclear reactor system. Nucl. Power Eng. **33**(3), 21–27 (2012). https://doi.org/10.3969/j.issn.0258-0926.2012.03.005 (**in Chinese**)
25. E. López-Honorato, J. Tan, P.J. Meadows et al., TRISO coated fuel particles with enhanced SiC properties. J. Nucl. Mater. **392**(2), 219–224 (2009). https://doi.org/10.1016/j.jnucmat.2009.03.013
26. R.Z. Liu, M.L. Liu, B. Liu et al., Design and preparation of SiC-based novel coated fuel particle. At. Energ. Sci. Technol. **50**(07), 1264–1269 (2016). https://doi.org/10.7538/yzk.2.16.50.07.1264 (**in Chinese**)
27. R. Yan, S.H. Yu, Y. Zou et al., Study on neutronics design of ordered-pebble-bed fluoride-salt-cooled high-temperature experimental reactor. Nucl. Sci. Tech. **29**, 81 (2018). https://doi.org/10.1007/s41365-018-0414-0
28. S.J. Liu, G.F. Zhu, R. Yan et al., Placement scheme of burnable poisons in a small modular fluoride-cooled high temperature reactor. Nucl. Tech. **43**, 050602 (2020). https://doi.org/10.11889/j.0253-3219.2020.hjs.43.050602
29. K.V.V. Devi, J.N. Dubey, J. Gupta et al., TRISO fuel volume fraction & homogeneity: A nondestructive characterization. Nucl. Sci. Tech. **30**, 41 (2019). https://doi.org/10.1007/s41365-019-0573-7
30. S.M. Bowman, Keno-vi Primer: a primer for criticality calculations with SCALE/KENO-VI using GEEWIZ. ORNL/TM-069 (2008)
31. G.F. Zhu, R. Yan, S.H. Yu et al., An application of direct statistical method for kinetics parameters in TMSR-SF1. Nucl. Tech. **41**, 050603 (2018). https://doi.org/10.11889/j.0253-3219.2018.hjs.41.050603 (**in Chinese**)